ACS APPLIED MATERIALS & INTERFACES

Research Article

www.acsami.org

Efficient Oxygen Reduction Electrocatalyst Based on Edge-Nitrogen-Rich Graphene Nanoplatelets: Toward a Large-Scale Synthesis

Xiaogang Fu, Jutao Jin, Yanru Liu, Zhiyang Wei, Fuping Pan, and Junyan Zhang*

State Key Laboratory of Solid Lubrication, Lanzhou Institute of Chemical Physics, Chinese Academy of Sciences, Lanzhou 730000, China

Supporting Information

ABSTRACT: The large-scale synthesis of nitrogen doped graphene (N-graphene) with high oxygen reduction reaction (ORR) performance has received a lot of attention recently. In this work, we have developed a facile and economical procedure for mass production of edge-nitrogen-rich graphene nanoplatelets (ENR-GNPs) by a combined process of ball milling of graphite powder (GP) in the presence of melamine and subsequent heat treatment. It is found that the ball milling process can not only crack and exfoliate pristine GP into edge-expanded nanoplatelets but also mechanically activate GP to generate appropriate locations for N-doping. Analysis results indicate that the doped N atoms mainly locate on the edge of the graphitic matrix, which contains ca. 3.1 at.% nitrogen content and can be well-dispersed in aqueous to form multilayer nanoplatelets. The as-prepared ENR-GNPs electrocatalyst exhibits highly electrocatalytic activity for ORR due to the synergetic effects of edge-N-doping and nanosized platelets. Besides, the stability and methanol tolerance of ENR-GNPs are superior to that of the commercial Pt/C catalyst, which makes the nanoplatelets a promising candidate for fuel cell cathode catalysts. The present approach opens up the possibility for simple and mass production of N-graphene based electrocatalysts in practice.

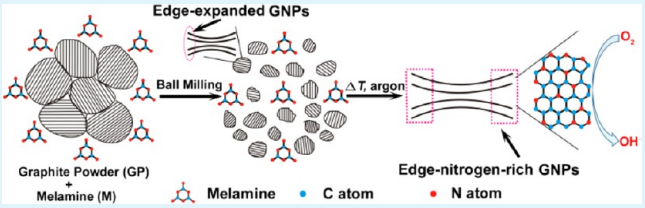

KEYWORDS: *Ball milling, edge-nitrogen-rich graphene, electrocatalyst, oxygen reduction reaction, fuel cell*

INTRODUCTION

Electrocatalysts for the oxygen reduction reaction (ORR) are key components of fuel cells, which significantly determine the cell performance and cost.[1,2] Platinum-based materials have been adopted as the most efficient catalysts for ORR and are still commonly used in commercial fuel cells owing to their relatively low overpotential and high current density.[3,4] However, the issues of prohibitive cost, scarce sources, methanol deactivation and weak durability extensively restrict their large-scale production and hamper the commercialization of fuel cells.[5−9] Accordingly, in the past decades, much attention has been devoted to explore non-noble catalysts to replace platinum-based catalysts. Currently, nitrogen-doped carbon materials are generally accepted as a potential substitute for platinum-based catalysts due to their high ORR activities, relatively low cost and excellent tolerance toward methanol.[10−17] Among these materials, nitrogen doped graphene (N-graphene), due to its efficient electrocatalytic activities, has attracted growing interest in the past few years.[18−22] Thus, extensive efforts have been made to synthesis of N-graphene for high efficient catalysts. Chemical vapor deposition (CVD) is the most common approach to prepare N-graphene films.[23−25] However, the extremely low yield and high cost limits the application of this method only to fundamental studies. The physicochemical exfoliation and reduction methods have been applied for bulk production of low cost N-graphene; however, the processes require the involvement of hazardous strong oxidizing and reduction reagents and a tedious multistep process.[26−28] Thus, the inherent costs and technical challenges of these traditional approaches inhibit the mass production of N-graphene and their application. On the other hand, the catalytic activity of these N-graphene catalysts is strongly linked to the location of the incorporated N in the graphene matrix, and it is reported that the doped-N atoms near the edge of the graphene sheets, in particular, act as the most desirable active sites for improved electrocatalytic activity.[29−31] Hence, it is therefore advantageous to develop a simple and economic strategy to prepare N-graphene on large-scale while containing more edge-doped-N for producing advanced electrocatalyst. Recently, the ball milling process has been used to prepare scalable quantities of graphene nanoplatelets.[32−34] In-Yup Jeon et al. have shown that ball mill graphite with N_2 can prepare nitrogenated graphene as electrocatalyst for energy conversion.[32] It could be suggested that ball milling is a very promising way for preparing functionalized graphene, however, in ordered to achieve a practical application there is much more to be done.

Herein, we describe a direct route toward edge-nitrogen-rich graphene nanoplatelets (ENR-GNPs) by simply dry ball milling graphite powder (GP) in the presence of melamine and followed by subsequent thermal treatment; meanwhile, the effects of ball milling and annealing on the ORR performance

Received: November 14, 2013
Accepted: February 21, 2014
Published: March 5, 2014

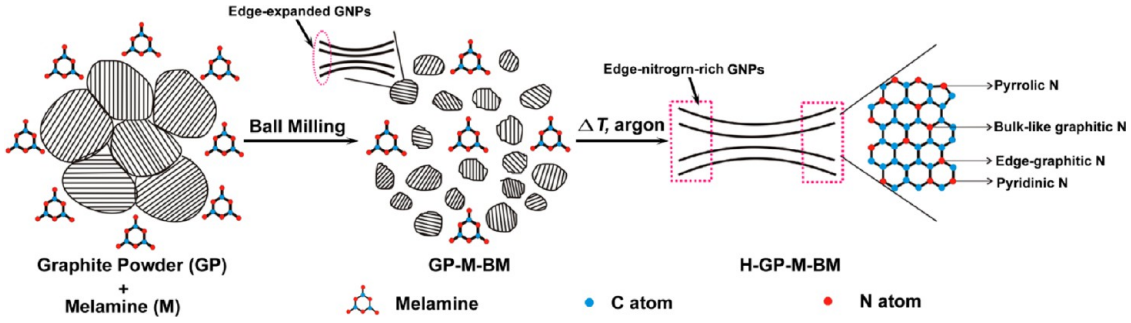

Figure 1. Schematic illustration of cracking and exfoliating of pristine GP by ball milling with melamine and subsequent pyrolysis resulted in the formation of edge-nitrogen-rich GNPs.

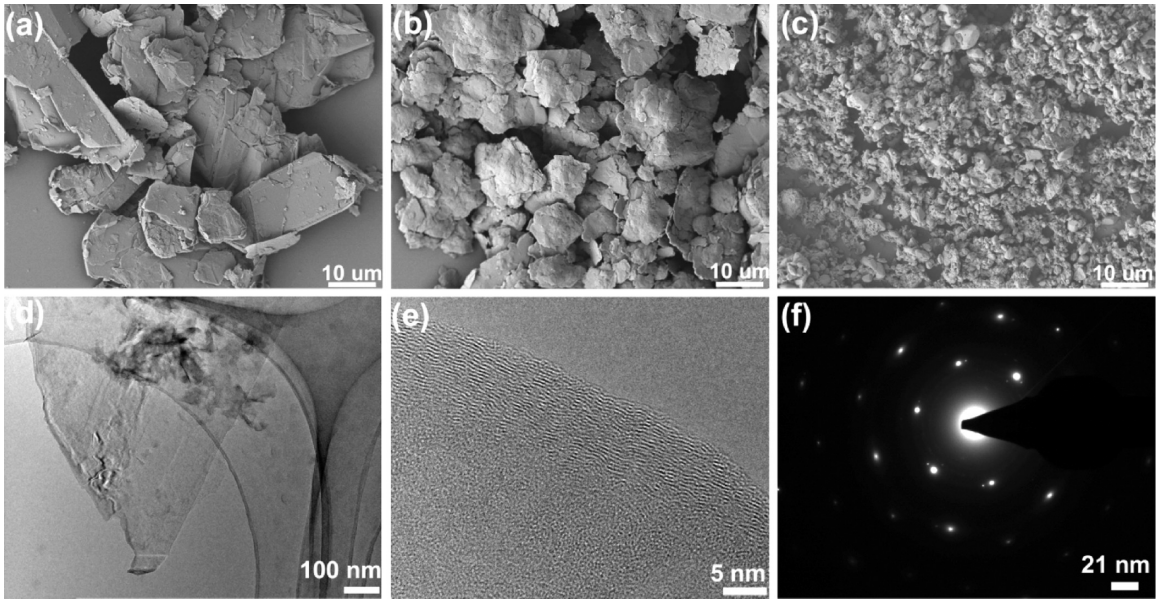

Figure 2. SEM images: (a) the pristine GP, (b) GP-BM and (c) GP-M-BM. TEM images: (d) GP-M-BM at low magnification, (e) GP-M-BM at high magnification and (f) the selected-area electron diffraction (SAED) pattern.

were also investigated. In this paper, ball milling is uniquely employed here to serve the following functions: (1) it used to crack and exfoliate parent GP into edge-expanded nanoplatelets, and (2) it can also mechanically activate these nanoplatelets to form more disordered phase at the edge of the graphitic matrix. The disordered phase helps incorporate nitrogen atoms into graphitic support on annealing in NH_3 atmosphere, which is important to form active sites for ORR.[35] In addition, melamine is used not only to help crack and exfoliate GP into edge-expanded nanoplatelets but also to act as a nitrogen source for the subsequent N-doping effect. The obtained ENR-GNPs with nitrogen content ca. 3.1 at.% can be well-dispersed in aqueous to form multilayer nanoplatelets. Due to the synergetic effects of edge-N-doping and nanosized platelets, the ENR-GNPs electrocatalyst exhibits excellent electrocatalytic activity, stability and methanol tolerance to the commercial Pt/C electrocatalyst for ORR in alkaline medium. The present approach opens up the possibility for simple and mass production of N-graphene based electrocatalysts with high ORR performance.

EXPERIMENTAL SECTION

General Procedure for the H-GP-M-BM. First, the GP-M-BM were prepared simply by ball milling of the pristine GP in a planetary ball mill machine (QM-3A, Nanda, China) in the presence of melamine.[36] To start with, 2 g of pristine GP, 6 g of melamine and 30 stainless steel balls (diameter = 5 mm) were put into a stainless steel capsule and sealed under air atmosphere. The ball milling was carried out at 500 rpm for 48 h. The resulted dark black powder (GP-M-BM) was further heat treated at 900 °C under an argon atmosphere for 2 h, which was referred to as "H-GP-M-BM". For comparison, GP-BM powder was prepared via ball milling in the absence of melamine and then heat treated with melamine to obtain "H-GP-BM-M".

Electrochemical Study. Electrochemical experiments were performed using an AutoLab workstation (μ Autolab III) with a typical three-electrode cell. A platinum wire and an Ag/AgCl electrode (saturated KCl filled) were used as the counter electrode and reference electrode, respectively. A glassy carbon (GC) electrode with a diameter of 3 mm covered by a thin film of the catalyst was used as the working electrode. Typically, 4 mg of ENR-GNPs was ultrasonically dispersed in a mixture of 0.8 mL of DI water, 0.2 mL of ethanol and 100 μL of 5 wt % Nafion solution. Then 5 μL of the homogeneous ink was drop-casted on the GC electrode surface (loading ~0.283 mg cm^{-2}) to afford ENR-GNPs/GC electrodes, followed by drying at room temperature. The other electrodes were prepared with the same approach. All electrochemical measurements were performed at room temperature either in 0.1 M KOH medium or 0.5 M H_2SO_4 medium, which were saturated with nitrogen or oxygen.

RESULTS AND DISCUSSION

For the facile and mass production of ENR-GNPs, first, edge-expanded GNPs were prepared via ball milling approach

dx.doi.org/10.1021/am405130w | ACS Appl. Mater. Interfaces 2014, 6, 3930−3936

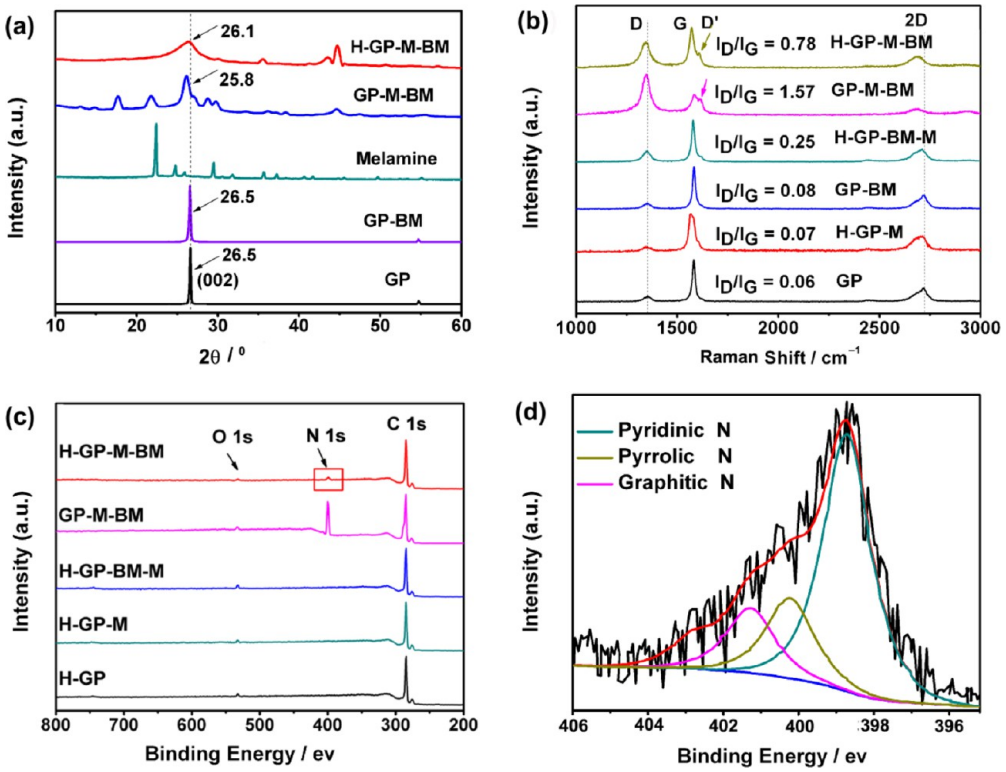

Figure 3. (a) XRD diffraction patterns, (b) Raman spectra, (c) XPS survey spectra and (d) High-resolution XPS N 1s spectra of H-GP-M-BM.

(Figure 1). This was achieved by ball milling (BM) of graphite powder (GP) and melamine (M) together through planetary ball milling machine, the resulted sample was denoted as GP-M-BM, see the Experimental Section for details. Because of the unique aminotriazines structure of melamine, it can strongly adsorb on graphite through hydrogen-bonding, thus promoting the crack and exfoliation of graphite.[36,37] This can be corroborated by the scanning electron microscopy (SEM) images of the ball milled samples without any postpurification or separation processes. As we can see, the pristine GP shows microscale (50 mesh, <270 um) irregular particle grains with smooth surfaces (Figure 2a). The ball milled pristine GP without melamine (denote as GP-BM) also shows microscale (~20 um) overlapped flakes (Figure 2b). As proposed in Figure 1, after ball milling through interactions with melamine, more homogeneous but much smaller grains (~500 nm) formed (Figure 2c and S1a, Supporting Information). It must be mentioned that the synthesis was not investigate the relationship between graphite size with ball milling duration, and all the samples were ball milled for 48 h as the same conditions.

GP-M-BM were dispersed in EtOH (Figure S1d, Supporting Information) for transmission electron microscopy (TEM) investigation. Figure 2d shows a TEM image of a representative multilayered and transparent nanoplatelets with winkled structures, which indicate their high degree of exfoliation. Under a higher magnification, the corresponding TEM image shows the thin film has some edge distortion and honeycomb-type morphologies for inner intact basal planes in Figure 2e. This edge distortion image indicates the occurrence of a significant edge-expansion in GP-M-BM, as schematically shown in Figure 1. The corresponding selected area electron diffraction (SAED) (Figure 2f) shows a typical 6-fold symmetry pattern, indicating high crystallinity of the GNPs. X-ray diffraction (XRD) patterns also prove the bulk GP can be smashed into edge-expanded nanoplatelets. As shown in Figure 3a, a characteristic and strong [002] peak appears at 26.5°, indicating a layer-to-layer *d*-spacing of 0.34 nm for pristine GP. After the ball milling process without melamine, there is only a slight change in the [002] peak of GP-BM compared with pristine GP, which indicates these overlapped flakes are nonexfoliated particles. Significantly, a broad peak with weaker intensity at 25.8° is observed for GP-M-BM, which implicates that the edges of GP-M-BM are exfoliated to a great extent. Hence, combined with the SEM, TEM and XRD results, it is found that the ball milling process can promote the crack and delamination of GP, which is a robust way to prepare multilayer GNPs.

Heat treatment of carbon materials with nitrogen source is considered an efficient approach to prepare N-doped materials.[38,39] Thus, in order to generate ENR-GNPs, the forementioned GP-M-BM nanocomposites were calcined at 900 °C under Ar for 2 h (that is H-GP-M-BM, Figure 1). In this stage, the unseparated melamine act as nitrogen sources for the N-doping process due to its high N content (66.7% by mass).[40,41] The use of ball milled graphite with melamine as precursors for the postsynthesis annealing allows for a low cost, large-scale production of ENR-GNPs, as shown in this work.

The as-prepared H-GP-M-BM also shows nanoscale (Figure S1b,c, Supporting Information), after sonicated in EtOH, the H-GP-M-BM can be further exfoliated into multilayer ENR-GNPs. TEM images also reveal that the dispersed ENR-GNPs have a significant tendency to coalesce into overlapped structures and are somewhat wrinkled on the grid (Figure S2, Supporting Information). Though the great mass of the obtained ENR-GNPs are multilayered materials, which are thicker than the ideal monolayer graphene, such a practical technique can provide the product in gram quantities.

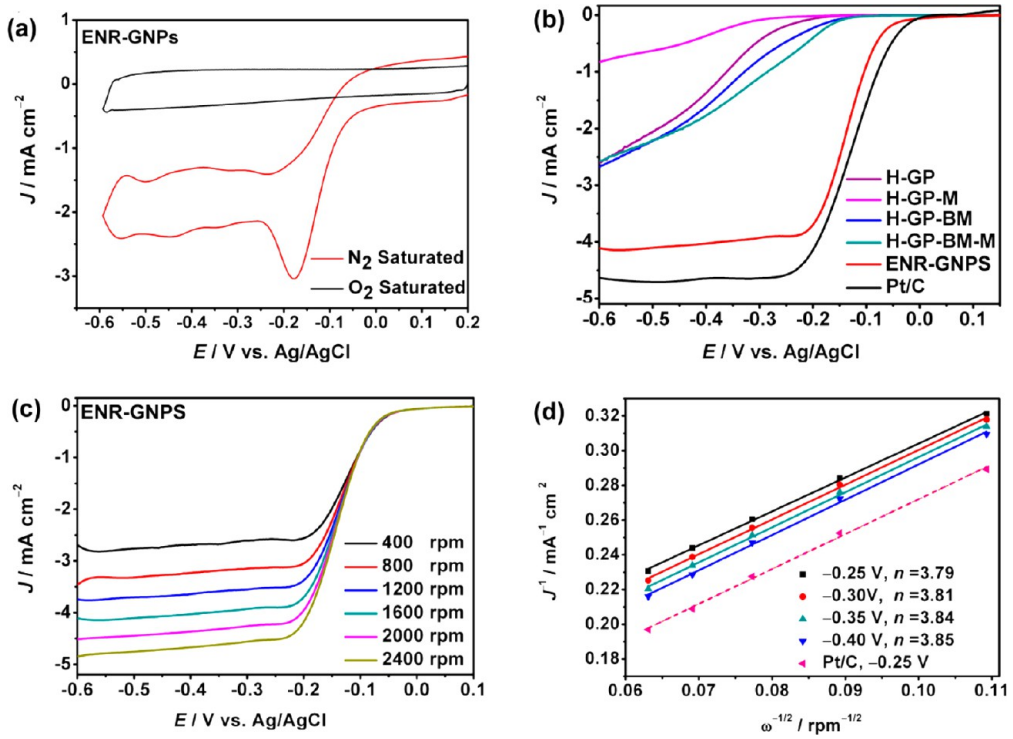

Figure 4. (a) Cyclic voltammograms of ENR-GNPs/GC electrode in N_2-saturated and O_2-saturated 0.1 M KOH solution at a scan rate of 50 mV s^{-1}. (b) LSV curves of samples/GC electrodes in O_2-saturated 0.1 M KOH solution at 1600 rpm with a scan rate of 5 mV s^{-1}. (c) Rotating disk electrode (RDE) voltammograms of ENR-GNPs/GC electrode in O_2-saturated 0.1 M KOH solution at a scan rate of 5 mV s^{-1} with different rotation rates from 400 to 2400 rpm. (d) Koutecky–Levich plots of ENR-GNPs at different electrode potentials.

Raman spectra were used to investigate the changes of the physical structure caused by ball milling and heat treatment. As can be seen in Figure 3b, the pristine GP shows a very weak D band at 1354 cm^{-1} owing to its bulk network (see Figure 2a), while, the G and 2D bands appear at 1580 and 2700 cm^{-1}, respectively.[42] Hence, the ratio of the D band to G band intensity (I_D/I_G) is very low and found to be approximately 0.06 (Figure 3b). The spectra changes are very slight for GP-BM compared with GP, and the low I_D/I_G ratio (0.08) indicates that ball milling without melamine cause negligible exfoliation and edge damage to GP-BM. Remarkable, upon ball milling with melamine, the GP-M-BM shows a strong D band over 1345 cm^{-1} with I_D/I_G = 1.57. The sharply enhanced intensity could be assigned to the significant edge-expansion and the increasement of disorder phase. In addition, D′ appears as a shoulder around 1600 cm^{-1} on the G band of GP-M-BM, which is also a characteristic of weak disorder on the graphitic structure.[34] According to previous reports, the more disordered phase in the pristine carbon, the easier for N-doping effect, because the disordered phase reacts faster with NH_3 than the graphitic phase during the heat treatment and help fix nitrogen atoms in the carbon structure.[35] Hence, the GP-M-BM sample is very favorable for N-doping. After heat treated the forementioned precursors mixed with melamine, there is nearly no change of the I_D/I_G ratio for H-GP-M (0.07) and slightly higher ratio for H-GP-BM-M (0.25), which indicates a few structure defects caused by heat treatment. Interestingly, the resulted H-GP-M-BM shows lower D band in comparison with this of GP-M-BM, and the I_D/I_G ratio for H-GP-M-BM decreases to 0.78. This result probably due to the graphitic basal plane structures of H-GP-M-BM have been restored during the heat-treatment. The XRD diffraction patterns also show that the [002] peak of H-GP-M-BM moves to 26.1° (Figure 3a), which further indicates the reassemble of graphitic basal plane. At the same time, the N-doping effect which could increase the intensity of D band should not be ignored.[19] Hence, the resulted I_D/I_G ratio for H-GP-M-BM could be the combined effects of basal plane restoration and N-doping.

Further evidence for the N-doping effect influenced by the ball milling process comes from the X-ray photoelectron spectroscopy (XPS) spectroscopic measurements. As shown in Figure 3c, the intermediate GP-M-BM shows a pronounced C 1s peak at around 284.8 eV, a weak O 1s peak at around 532 eV and a sharp N 1s peak locates at around 400 eV arising from melamine. Upon heat treatment, in addition to the O 1s and C 1s peaks, the H-GP-M-BM shows a noticeable N 1s peak, which is very different from GP-M-BM, indicating that an amount of nitrogen has been covalently doped into H-GP-M-BM. The further XPS analysis (Table S1, Supporting Information) reveals the presence of ca. 3.1 at.% nitrogen in the H-GP-M-BM, and this value is lower than that from traditional methods (ca. 4.0 at.% from CVD,[24] ca. 8.1 at.% from N-doped graphene oxide).[41] However, none of the heat treated control samples show the detected N1s peak in the XPS spectrum (Figure 3c). The absence of N in these control samples indicates that the foreign N atoms may have not been incorporated into the graphitic framework. In other words, ball milled GP with melamine together is an indispensable pretreatment for the subsequent N-doping procedure. This is because only in the presence of melamine can the GP be cracked and exfoliated to nanoscale platelets with more disordered phase, namely the ball milling process could promote the graphitic matrix generate more appropriate locations for N-doping. Given that the present approach offers GNPs without basal plane distortion

dx.doi.org/10.1021/am405130w | ACS Appl. Mater. Interfaces 2014, 6, 3930−3936

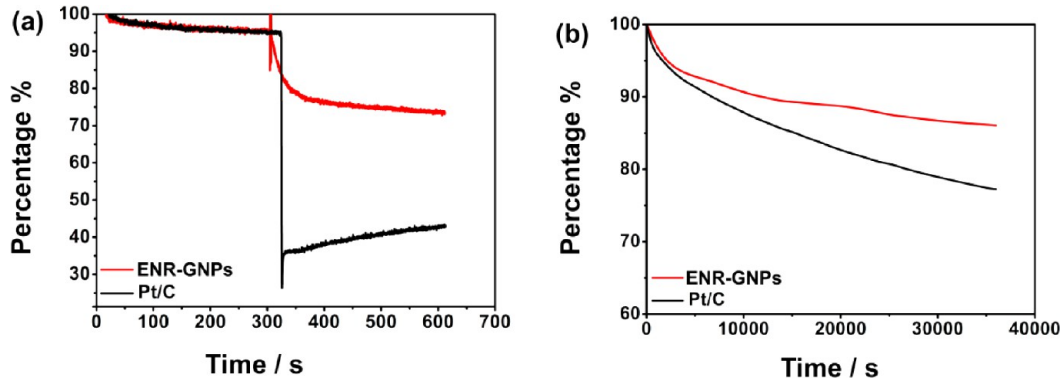

Figure 5. Current−time (i−t) chronoamperometric response of ENR-GNPs and Pt/C electrodes at −0.30 V in O_2-saturated 0.1 M KOH solution with a rotation rate of 1600 rpm: (a) upon addition of 3 M methanol after 300 s and (b) durability evaluation for 36 000 s.

(Figure 2e), it is inferred that the disordered carbon could mainly exist on the edge-expanded area of the graphitic matrix. Consequently, the nitrogen atoms would prefer to be incorporated into the edge of the graphite matrix to form edge-nitrogen-rich nanoplatelets. The high-resolution N 1s scan for H-GP-M-BM (Figure 3d) indicates the edge nitrogen could be assigned to three species: pyridinic N (~398.1 eV), pyrrolic N (~400.2 eV) and graphitic N (~401.2 eV).[43] While the pyridinic N and pyrrolic N always locate on the edge of the graphite matrix and graphitic N can be both edge-graphitic N and bulk-like-graphitic N (Figure 1). Though all these nitrogen forms have been shown to serve as catalytically active sites for ORR,[44] it is proposed that the outermost graphitic nitrogen sites (edge-graphitic N) among others are the main active sites due to the lowest barrier for electron transfer as well as the highest selectivity toward the four-electron reduction pathway.[29] Moreover, the pyridinic N could also act as a marker for edge plane exposure, so the dominant pyridinic N (56% atomic concentration among all N components) indicates the H-GP-M-BM has abundant edge plane and therefore a higher proportion of more active edge-graphitic N. As expected, the obtained ENR-GNPs electrocatalyst could show excellent ORR activity (see below).

The electrocatalytic activity of ENR-GNPs electrode was first assessed by cyclic voltammetry (CV) in 0.1 M KOH solution saturated with nitrogen or oxygen at a scan rate of 50 mV s^{-1} (Figure 4a). In the nitrogen-saturated solution, featureless voltammetric currents are observed between −0.6 and +0.2 V. In contrast, when the electrolyte solution is saturated with oxygen, a well-defined cathodic peak at −0.17 V is clearly observed, which confirms that the ENR-GNPs electrode exhibits pronounced electrocatalytic activity for ORR. To further investigate the electrocatalytic activity of these obtained samples, linear sweep voltammetric (LSV) measurements were performed on a rotating disk electrode (RDE) in oxygen-saturated 0.1 M KOH at a rotation speed of 1600 rpm (Figure 4b). It is obvious that only the ENR-GNPs electrode exhibits a substantial oxygen reduction process, the onset potentials of ORR is more positive and the current density is much higher than other electrodes with negligible ORR catalytic activity. What's more, the half-wave potential ($E_{1/2}$) of ENR-GNPs electrode is only 12 mV negative shift compared with Pt/C catalyst. This is mainly due to the N-doping effect, which can sharply enhance the ORR activity of graphitic materials, because only the sample prepared as Figure 1 shows detected nitrogen content. According to previous reports, the overall nitrogen content may significantly influence the performance of ORR catalysis.[45,46] However, despite the N-graphene nanoplatelets prepared in this study have lower N-doping level than that from traditional methods, the ORR performance is excellent and even approaching that of the commercial Pt/C catalyst. It is likely that the unique structure of edge-nitrogen-rich GNPs could account for the high ORR activity. Above all, due to the edge-N-doping effect, the incorporated nitrogen atoms mainly locate on the edge of the graphitic matrix, which could generate more active sites for ORR. Moreover, compared to the traditional approaches, the ball milling process could avoid introducing abundant defects into graphitic matrix and keep intact of their inner basal planes, which can retain their electrical conductivity to facilitate charge transport during electrocatalysis. In addition to the edge-N-doping effect, the nanosized platelets could also contribute to the pronounced ORR performance. On one hand, ball milling process can result in nanosized graphene nanoplatelets with more active zigzag edges which could improve the activation of oxygen and therefore promote the ORR activity.[47] On the other hand, the reduced size of ENR-GNPs could sharply enhance the Brunauer−Emmett−Teller (BET) specific surface area (Figure S3, Supporting Information), which can expose more edge active sites to electrolytes and thus result in ORR activity enhancement. As mentioned above, this high ORR activity could be the synergetic effects of edge-N-doping and nanosized platelets. The above analysis further indicates that ball milling process play an important role to the high ORR activity.

RDE measurements at various rotating speeds are also performed to gain further insight into the kinetics of the ORR at the ENR-GNPs electrode (Figure 4c). It can be seen that there was a simultaneous increase of the limited diffusion current density along with the rotating rates, owing to the shorted diffusion layer.[48] The Koutecky−Levich plots (j^{-1} vs $\omega^{-1/2}$, Figure 4d) at different potentials show fine linearity and parallelism, indicating first-order reaction kinetics for ORR with respect to the concentration of dissolved oxygen.[49] According to the Koutecky−Levich equation (eqs 1 and 2, Supporting Information),[50] the electron transfer number (n) of ORR is calculated to be 3.82 at potentials from −0.40 to −0.25 V, suggesting that ENR-GNPs catalyst exhibits dominant 4 electron oxygen reduction process similar to the commercial Pt/C catalyst (Figure S4, Supporting Information).

The ENR-GNPs electrode is further subjected to testing the methanol tolerance ability and the electrochemical stability toward ORR via a current−time (i−t) chronoamperometric

method. As shown in Figure 5a, the original cathodic current of ENR-GNPs electrode reduces slightly after the addition of methanol into the electrolyte solution. In contrast, the corresponding current on commercial Pt/C electrode decreases sharply upon addition methanol. This result unambiguously suggests that the ENR-GNPs electrocatalyst exhibits better methanol tolerance than the commercial Pt/C electrocatalyst. Subsequently, the continuous oxygen reduction in oxygen-saturated 0.1 M KOH solutions clearly demonstrates that the stability of ENR-GNPs catalyst is superior to that of the commercial Pt/C catalyst (Figure 5b). Furthermore, the ENR-GNPs catalyst also exhibits remarkable ORR activity under acidic conditions (0.5 M H_2SO_4, Figure S5, Supporting Information).

CONCLUSIONS

In summary, we have developed a direct route to large-scale production of ENR-GNPs by dry ball milling graphite powder with melamine and followed by subsequent thermal treatment. The ball milling process plays a very important role in this approach, including preparing graphene nanoplatelets, facilitating the N-doping effect and enhancing the ORR activity. The as prepared ENR-GNPs with ca. 3.1 at.% nitrogen content can be highly dispersed to form multilayer nanoplatelets. Further analysis results indicate that the doped N atoms mainly locate on the edge of the graphitic matrix, and the edge-graphitic N may have a higher proportion. Due to the synergetic effects of edge-N-doping and nanosized platelets, the ENR-GNPs electrode exhibits excellent ORR activity in alkaline electrolytes, and its half-wave potential ($E_{1/2}$) is only 12 mV negative shift compared with commercial Pt/C catalyst. What's more, compared to a commercial Pt/C catalyst, the ENR-GNPs electrode shows superior stability and methanol tolerance. Given that this preparation technique utilizes cheap precursors and does not require hazardous solvents, vacuum systems or tedious post treatment, this facile low cost approach to mass production of high efficient N-graphene based electrocatalyst can be achieved in practice.

ASSOCIATED CONTENT

Supporting Information

A detailed RDE electrochemical measurements and characterization; SEM, TEM, BET of H-GP-M-BM; RDE voltammograms and Koutecky–Levich plot of Pt/C; XPS analysis date for atom composition. This material is available free of charge via the Internet at http://pubs.acs.org.

AUTHOR INFORMATION

Corresponding Author

*J. Zhang. E-mail: zhangjunyan@licp.cas.cn.

Notes

The authors declare no competing financial interest.

ACKNOWLEDGMENTS

This work was supported by National Nature Science Foundation of China (Grant No. 50823008).

REFERENCES

(1) Bashyam, R.; Zelenay, P. A Class of Non-Precious Metal Composite Catalysts for Fuel Cells. *Nature* **2006**, *443*, 63–66.
(2) Jasinski, R. A New Fuel Cell Cathode Catalyst. *Nature* **1964**, *201*, 1212–1213.
(3) Stamenkovic, V. R.; Fowler, B.; Mun, B. S.; Wang, G.; Ross, P. N.; Lucas, C. A.; Marković, N. M. Improved Oxygen Reduction Activity on $Pt_3Ni(111)$ via Increased Surface Site Availability. *Science* **2007**, *315*, 493–497.
(4) Guo, S.; Dong, S.; Wang, E. Three-Dimensional Pt-on-Pd Bimetallic Nanodendrites Supported on Graphene Nanosheet: Facile Synthesis and Used as an Advanced Nanoelectrocatalyst for Methanol Oxidation. *ACS Nano* **2010**, *4*, 547–555.
(5) Chen, S.; Wei, Z.; Qi, X.; Dong, L.; Guo, Y. G.; Wan, L.; Shao, Z.; Li, L. Nanostructured Polyaniline-Decorated Pt/C@PANI Core-Shell Catalyst with Enhanced Durability and Activity. *J. Am. Chem. Soc.* **2012**, *134*, 13252–13255.
(6) Marković, N. M.; Schmidt, T. J.; Stamenković, V.; Ross, P. N. Oxygen Reduction Reaction on Pt and Pt Bimetallic Surfaces: A Selective Review. *Fuel Cells* **2001**, *1*, 105–116.
(7) Sun, S.; Zhang, G.; Geng, D.; Chen, Y.; Li, R.; Cai, M.; Sun, X. A Highly Durable Platinum Nanocatalyst for Proton Exchange Membrane Fuel Cells: Multiarmed Starlike Nanowire Single Crystal. *Angew. Chem., Int. Ed.* **2011**, *50*, 422–426.
(8) Mazumder, V.; Chi, M.; More, K. L.; Sun, S. Core/Shell Pd/FePt Nanoparticles as an Active and Durable Catalyst for the Oxygen Reduction Reaction. *J. Am. Chem. Soc.* **2010**, *132*, 7848–7849.
(9) Sebastián, D.; Ruíz, A. G.; Suelves, I.; Moliner, R.; Lázaro, M. J.; Baglio, V.; Stassi, A.; Aricò, A. S. Enhanced Oxygen Reduction Activity and Durability of Pt Catalysts Supported on Carbon Nanofibers. *Appl. Catal., B* **2012**, *115–116*, 269–275.
(10) Rao, C. V.; Cabrera, C. R.; Ishikawa, Y. In Search of the Active Site in Nitrogen-Doped Carbon Nanotube Electrodes for the Oxygen Reduction Reaction. *J. Phys. Chem. Lett.* **2010**, *1*, 2622–2627.
(11) Soin, N.; Roy, S.; Sharma, S.; Thundat, T.; McLaughlin, J. Electrochemical and Oxygen Reduction Properties of Pristine and Nitrogen-Doped Few Layered Graphene Nanoflakes (FLGs). *J. Solid State Electrochem.* **2013**, *17*, 2139–2149.
(12) Chen, Z. W.; Higgins, D.; Yu, A. P.; Zhang, L.; Zhang, J. J. A Review on Non-Precious Metal Electrocatalysts for PEM Fuel Cells. *Energy Environ. Sci.* **2011**, *4*, 3167–3192.
(13) Jaouen, F.; Proietti, E.; Lefevre, M.; Chenitz, R.; Dodelet, J. P.; Wu, G.; Chung, H. T.; Johnston, C. M.; Zelenay, P. Recent Advances in Non-Precious Metal Catalysis for Oxygen-Reduction Reaction in Polymer Electrolyte Fuel Cells. *Energy Environ. Sci.* **2011**, *4*, 114–130.
(14) Wiggins-Camacho, J. D.; Stevenson, K. J. Mechanistic Discussion of the Oxygen Reduction Reaction at Nitrogen-Doped Carbon Nanotubes. *J. Phys. Chem. C* **2011**, *115*, 20002–20010.
(15) Jaouen, F. d. r.; Herranz, J.; Lefèvre, M.; Dodelet, J.-P.; Kramm, U. I.; Herrmann, I.; Bogdanoff, P.; Maruyama, J.; Nagaoka, T.; Garsuch, A.; Dahn, J. R.; Olson, T.; Pylypenko, S.; Atanassov, P.; Ustinov, E. A. Cross-Laboratory Experimental Study of Non-Noble-Metal Electrocatalysts for the Oxygen Reduction Reaction. *ACS Appl. Mater. Interfaces* **2009**, *1*, 1623–1639.
(16) Rao, C. V.; Ishikawa, Y. Activity, Selectivity, and Anion-Exchange Membrane Fuel Cell Performance of Virtually Metal-Free Nitrogen-Doped Carbon Nanotube Electrodes for Oxygen Reduction Reaction. *J. Phys. Chem. C* **2012**, *116*, 4340–4346.
(17) Wiggins-Camacho, J. D.; Stevenson, K. J. Effect of Nitrogen Concentration on Capacitance, Density of States, Electronic Conductivity, and Morphology of N-Doped Carbon Nanotube Electrodes. *J. Phys. Chem. C* **2009**, *113*, 19082–19090.
(18) Shao, Y.; Zhang, S.; Engelhard, M. H.; Li, G.; Shao, G.; Wang, Y.; Liu, J.; Aksay, I. A.; Lin, Y. Nitrogen-Doped Graphene and Its Electrochemical Applications. *J. Mater. Chem.* **2010**, *20*, 7491–7496.
(19) Wang, H.; Maiyalagan, T.; Wang, X. Review on Recent Progress in Nitrogen-Doped Graphene: Synthesis, Characterization, and Its Potential Applications. *ACS Catal.* **2012**, *2*, 781–794.
(20) Fu, X.; Liu, Y.; Cao, X.; Jin, J.; Liu, Q.; Zhang, J. FeCo–Nx Embedded Graphene as High Performance Catalysts for Oxygen Reduction Reaction. *Appl. Catal., B* **2013**, *130–131*, 143–151.
(21) Jin, J.; Fu, X.; Liu, Q.; Zhang, J. A Highly Active and Stable Electrocatalyst for the Oxygen Reduction Reaction Based on a

Graphene-Supported g-C3N4@Cobalt Oxide Core-Shell Hybrid in Alkaline Solution. *J. Mater. Chem. A* **2013**, *1*, 10538−10545.
(22) Pan, F.; Jin, J.; Fu, X.; Liu, Q.; Zhang, J. Advanced Oxygen Reduction Electrocatalyst Based on Nitrogen-Doped Graphene Derived from Edible Sugar and Urea. *ACS Appl. Mater. Interfaces* **2013**, *5*, 11108−11114.
(23) Wei, D.; Liu, Y.; Wang, Y.; Zhang, H.; Huang, L.; Yu, G. Synthesis of N-Doped Graphene by Chemical Vapor Deposition and Its Electrical Properties. *Nano Lett.* **2009**, *9*, 1752−1758.
(24) Qu, L.; Liu, Y.; Baek, J. B.; Dai, L. Nitrogen-Doped Graphene as Efficient Metal-Free Electrocatalyst for Oxygen Reduction in Fuel Cells. *ACS Nano* **2010**, *4*, 1321−1326.
(25) Li, X.; Cai, W.; An, J.; Kim, S.; Nah, J.; Yang, D.; Piner, R.; Velamakanni, A.; Jung, I.; Tutuc, E.; Banerjee, S. K.; Colombo, L.; Ruoff, R. S. Large-Area Synthesis of High-Quality and Uniform Graphene Films on Copper Foils. *Science* **2009**, *324*, 1312−1314.
(26) Hummers, W. S.; Offeman, R. E. Preparation of Graphitic Oxide. *J. Am. Chem. Soc.* **1958**, *80*, 1339−1339.
(27) Niyogi, S.; Bekyarova, E.; Itkis, M. E.; McWilliams, J. L.; Hamon, M. A.; Haddon, R. C. Solution Properties of Graphite and Graphene. *J. Am. Chem. Soc.* **2006**, *128*, 7720−7721.
(28) Li, D.; Muller, M. B.; Gilje, S.; Kaner, R. B.; Wallace, G. G. Processable Aqueous Dispersions of Graphene Nanosheets. *Nat. Nanotechnol.* **2008**, *3*, 101−105.
(29) Kim, H.; Lee, K.; Woo, S. I.; Jung, Y. On the Mechanism of Enhanced Oxygen Reduction Reaction in Nitrogen-Doped Graphene Nanoribbons. *Phys. Chem. Chem. Phys.* **2011**, *13*, 17505−17510.
(30) Biddinger, E. J.; Ozkan, U. S. Role of Graphitic Edge Plane Exposure in Carbon Nanostructures for Oxygen Reduction Reaction. *J. Phys. Chem. C* **2010**, *114*, 15306−15314.
(31) Ikeda, T.; Boero, M.; Huang, S.-F.; Terakura, K.; Oshima, M.; Ozaki, J.-I. Carbon Alloy Catalysts: Active Sites for Oxygen Reduction Reaction. *J. Phys. Chem. C* **2008**, *112*, 14706−14709.
(32) Jeon, I.-Y.; Choi, H.-J.; Ju, M. J.; Choi, I. T.; Lim, K.; Ko, J.; Kim, H. K.; Kim, J. C.; Lee, J.-J.; Shin, D.; Jung, S.-M.; Seo, J.-M.; Kim, M.-J.; Park, N.; Dai, L.; Baek, J.-B. Direct Nitrogen Fixation at the Edges of Graphene Nanoplatelets as Efficient Electrocatalysts for Energy Conversion. *Sci. Rep.* **2013**, *3*, DOI: 10.1038/srep02260.
(33) Jeon, I.-Y.; Shin, Y.-R.; Sohn, G.-J.; Choi, H.-J.; Bae, S.-Y.; Mahmood, J.; Jung, S.-M.; Seo, J.-M.; Kim, M.-J.; Wook Chang, D.; Dai, L.; Baek, J.-B. Edge-Carboxylated Graphene Nanosheets via Ball Milling. *Proc. Natl. Acad. Sci. U. S. A.* **2012**, *109*, 5588−5593.
(34) Jeon, I.-Y.; Choi, H.-J.; Jung, S.-M.; Seo, J.-M.; Kim, M.-J.; Dai, L.; Baek, J.-B. Large-Scale Production of Edge-Selectively Functionalized Graphene Nanoplatelets via Ball Milling and Their Use as Metal-Free Electrocatalysts for Oxygen Reduction Reaction. *J. Am. Chem. Soc.* **2012**, *135*, 1386−1393.
(35) Jaouen, F.; Charreteur, F.; Dodelet, J. P. Fe-Based Catalysts for Oxygen Reduction in PEMFCs: Importance of the Disordered Phase of the Carbon Support. *J. Electrochem. Soc.* **2006**, *153*, A689−A698.
(36) Leon, V.; Quintana, M.; Herrero, M. A.; Fierro, J. L. G.; Hoz, A. d. l.; Prato, M.; Vazquez, E. Few-Layer Graphenes From Ball-Milling of Graphite with Melamine. *Chem. Commun.* **2011**, *47*, 10936−10938.
(37) Wuest, J. D.; Rochefort, A. Strong Adsorption of Aminotriazines on Graphene. *Chem. Commun.* **2010**, *46*, 2923−2925.
(38) Li, X.; Wang, H.; Robinson, J. T.; Sanchez, H.; Diankov, G.; Dai, H. Simultaneous Nitrogen Doping and Reduction of Graphene Oxide. *J. Am. Chem. Soc.* **2009**, *131*, 15939−15944.
(39) Su, D. S.; Sun, G. Nonprecious-Metal Catalysts for Low-Cost Fuel Cells. *Angew. Chem., Int. Ed.* **2011**, *50*, 11570−11572.
(40) Sheng, Z.-H.; Shao, L.; Chen, J.-J.; Bao, W.-J.; Wang, F.-B.; Xia, X.-H. Catalyst-Free Synthesis of Nitrogen-Doped Graphene via Thermal Annealing Graphite Oxide with Melamine and Its Excellent Electrocatalysis. *ACS Nano* **2011**, *5*, 4350−4358.
(41) Lin, Z.; Song, M.-k.; Ding, Y.; Liu, Y.; Liu, M.; Wong, C.-P. Facile Preparation of Nitrogen-Doped Graphene as a Metal-free Catalyst for Oxygen Reduction Reaction. *Phys. Chem. Chem. Phys.* **2012**, *14*, 3381−3387.
(42) Posudievsky, O. Y.; Khazieieva, O. A.; Koshechko, V. G.; Pokhodenko, V. D. Preparation of Graphene Oxide by Solvent-Free Mechanochemical Oxidation of Graphite. *J. Mater. Chem.* **2012**, *22*, 12465−12467.
(43) Pels, J. R.; Kapteijn, F.; Moulijn, J. A.; Zhu, Q.; Thomas, K. M. Evolution of Nitrogen Functionalities in Carbonaceous Materials During Pyrolysis. *Carbon* **1995**, *33*, 1641−1653.
(44) Gong, K.; Du, F.; Xia, Z.; Durstock, M.; Dai, L. Nitrogen-Doped Carbon Nanotube Arrays with High Electrocatalytic Activity for Oxygen Reduction. *Science* **2009**, *323*, 760−764.
(45) Lee, D. H.; Lee, W. J.; Kim, S. O. Highly Efficient Vertical Growth of Wall-Number-Selected, N-Doped Carbon Nanotube Arrays. *Nano Lett.* **2009**, *9*, 1427−1432.
(46) Lee, S. H.; Lee, D. H.; Lee, W. J.; Kim, S. O. Tailored Assembly of Carbon Nanotubes and Graphene. *Adv. Funct. Mater.* **2011**, *21*, 1338−1354.
(47) Deng, D.; Yu, L.; Pan, X.; Wang, S.; Chen, X.; Hu, P.; Sun, L.; Bao, X. Size Effect of Graphene on Electrocatalytic Activation of Oxygen. *Chem. Commun.* **2011**, *47*, 10016−10018.
(48) Yang, W.; Fellinger, T.-P.; Antonietti, M. Efficient Metal-Free Oxygen Reduction in Alkaline Medium on High-Surface-Area Mesoporous Nitrogen-Doped Carbons Made from Ionic Liquids and Nucleobases. *J. Am. Chem. Soc.* **2010**, *133*, 206−209.
(49) Ma, G.; Jia, R.; Zhao, J.; Wang, Z.; Song, C.; Jia, S.; Zhu, Z. Nitrogen-Doped Hollow Carbon Nanoparticles with Excellent Oxygen Reduction Performances and Their Electrocatalytic Kinetics. *J. Phys. Chem. C* **2011**, *115*, 25148−25154.
(50) Byon, H. R.; Suntivich, J.; Shao-Horn, Y. Graphene-Based Non-Noble-Metal Catalysts for Oxygen Reduction Reaction in Acid. *Chem. Mater.* **2011**, *23*, 3421−3428.